



Cite this: DOI: 10.1039/d1dt01770e

# Enhancing the barrier height for magnetization reversal in 4d/4f Ru<sup>III</sup>Ln<sup>III</sup> “butterfly” single molecule magnets (Ln = Gd, Dy) via targeted structural alterations†

Abinash Swain,<sup>a</sup> Robert Martin,<sup>b</sup> Kuduva R. Vignesh,<sup>id</sup><sup>a</sup> Gopalan Rajaraman,<sup>id</sup><sup>\*a</sup> Keith S. Murray<sup>id</sup><sup>\*c</sup> and Stuart K. Langley<sup>\*b</sup>

A series of 4d–4f {Ru<sup>III</sup>Dy<sup>III</sup>} and {Ru<sup>III</sup>Gd<sup>III</sup>} ‘butterfly’ (rhombohedral) complexes have been synthesized and characterized and their magnetic properties investigated. Earlier, we have reported the first 4d/4f SMM – [Ru<sup>III</sup>Dy<sup>III</sup>(OMe)<sub>2</sub>(O<sub>2</sub>CPh)<sub>4</sub>(mdea)<sub>2</sub>(NO<sub>3</sub>)<sub>2</sub>] (**1<sub>Dy</sub>**) with a  $U_{\text{eff}}$  value of 10.7 cm<sup>-1</sup>. As the structural distortion around the Dy<sup>III</sup> centres and the Ru<sup>III</sup>...Dy<sup>III</sup> exchange interactions are key to enhancing the anisotropy, in this work we have synthesised three more {Ru<sub>2</sub>Dy<sub>2</sub>} butterfly complexes where structural alteration around the Dy<sup>III</sup> centres and alterations to the bridging groups are performed with an aim to improve the magnetic properties. The new complexes reported here are [Ru<sub>2</sub>Dy<sub>2</sub>(OMe)<sub>2</sub>(O<sub>2</sub>C(4-Me-Ph)<sub>4</sub>(mdea)(MeOH)<sub>4</sub>], **2<sub>Dy</sub>**, [Ru<sub>2</sub>Dy<sub>2</sub>(OMe)<sub>2</sub>(O<sub>2</sub>C(2-Cl,4,5-F-Ph)<sub>4</sub>(mdea)<sub>2</sub>(NO<sub>3</sub>)<sub>2</sub>], **3<sub>Dy</sub>**, and an acac derivative [Ru<sub>2</sub>Dy<sub>2</sub>(OMe)<sub>2</sub>(acac)<sub>4</sub>(NO<sub>3</sub>)<sub>2</sub>(edea)<sub>2</sub>], **4<sub>Dy</sub>**, where acac<sup>-</sup> = acetylacetonate, edea<sup>2-</sup> = *N*-ethyl-diethanolamine dianion. Complex **2<sub>Dy</sub>** describes alteration in the Dy<sup>III</sup> centers, while complexes **3<sub>Dy</sub>** and **4<sub>Dy</sub>** are aimed to alter the Ru<sup>III</sup>...Dy<sup>III</sup> exchange pathways. To ascertain the 4d–4f exchange, the Gd-analogues of **1<sub>Dy</sub>** and **4<sub>Dy</sub>** were synthesised [Ru<sub>2</sub>Gd<sub>2</sub>(OMe)<sub>2</sub>(O<sub>2</sub>CPh)<sub>4</sub>(mdea)<sub>2</sub>(NO<sub>3</sub>)<sub>2</sub>], **1<sub>Gd</sub>**, [Ru<sub>2</sub>Gd<sub>2</sub>(OMe)<sub>2</sub>(acac)<sub>4</sub>(NO<sub>3</sub>)<sub>2</sub>(edea)<sub>2</sub>], **4<sub>Gd</sub>**. Both ac and dc susceptibility studies were performed on all these complexes, and out-of-phase signals were observed for **3<sub>Dy</sub>** in zero-field while **2<sub>Dy</sub>** and **4<sub>Dy</sub>** show out-of-phase signals in the presence of an applied field. Complex **3<sub>Dy</sub>** reveals a barrier height  $U_{\text{eff}}$  of 45 K. To understand the difference in the magnetic dynamic behavior compared to our earlier reported {Ru<sup>III</sup>Dy<sup>III</sup>} analogue, detailed theoretical calculations based on *ab initio* CASSCF/RASSI-SO calculations have been performed. Calculations reveal that the  $J_{\text{Ru}...Dy}$  value varies from -1.8 cm<sup>-1</sup> (**4<sub>Dy</sub>**) to -2.4 cm<sup>-1</sup> (**3<sub>Dy</sub>**). These values are also affirmed by DFT calculations performed on the corresponding Gd<sup>III</sup> analogues. The origin of the largest barrier and observation of slow magnetic relaxation in **3<sub>Dy</sub>** is routed back to the stronger single-ion anisotropy and stronger  $J_{\text{Ru}...Dy}$  exchange which quenches the QTM effects more efficiently. This study thus paves the way forward to tune local structure around the Ln<sup>III</sup> center and the exchange pathway to enhance the SMM characteristics in other {3d–4f}/(4d–4f) SMMs.

Received 31st May 2021,  
Accepted 7th August 2021  
DOI: 10.1039/d1dt01770e

rsc.li/dalton

## Introduction

Magnetic exchange interactions play a significant role in quenching the quantum tunnelling to improve the single

molecule magnet (SMM)<sup>1</sup> property of a molecule. This has become a crucial parameter in enhancing the SMM property for polynuclear systems.<sup>2</sup> The magnetic exchange coupling between the metal ion can be substantially enhanced either by using radical bridges or by suitable combination of specific metal ions.<sup>3,4</sup> Heterometallic 3d/4f compounds have developed into a key area of single molecule magnet research,<sup>4–6</sup> in particular examples such as tetranuclear [Cr<sup>III</sup>Dy<sup>III</sup>(OMe)<sub>2</sub>(O<sub>2</sub>CPh)<sub>4</sub>(mdea)<sub>2</sub>(NO<sub>3</sub>)<sub>2</sub>]<sup>7</sup> (mdea<sup>2-</sup> is *N*-methyl-diethanolamine dianion) butterfly complexes, display well resolved, highly coercive hysteresis loops, between 1.8–3.5 K at a sweep rate of 0.003 T s<sup>-1</sup>, as well as frequency dependent ac out-of-phase susceptibility ( $\chi''_{\text{M}}$ ) maxima ( $U_{\text{eff}} = 54$  cm<sup>-1</sup>) over the entire temperature range studied (4.5–10 K). This revealed

<sup>a</sup>Department of Chemistry, Indian Institute of Technology Bombay, Mumbai-400076, India. E-mail: rajaraman@chem.iitb.ac.in

<sup>b</sup>School of Science and the Environment, Division of Chemistry, Manchester Metropolitan University, Manchester, M15 6BH, UK. E-mail: s.langley@mmu.ac.uk

<sup>c</sup>School of Chemistry, 17 Rainforest Walk, Monash University, Clayton, Victoria 3800, Australia. E-mail: keith.murray@monash.edu

† Electronic supplementary information (ESI) available: Additional molecular structures, structural parameter tables, magnetic plots and calculated values. CCDC 2085827–2085831. For ESI and crystallographic data in CIF or other electronic format see DOI: 10.1039/d1dt01770e

quantum tunnelling of magnetisation (QTM) often seen for Ln<sup>III</sup> based SMMs was not the dominant relaxation process for this system, a key result in the quest for better performing SMMs. The Co<sup>III</sup> analogues, [Co<sup>III</sup>Dy<sup>III</sup>(OMe)<sub>2</sub>(O<sub>2</sub>CPh)<sub>4</sub>(mdea)<sub>2</sub>(NO<sub>3</sub>)<sub>2</sub>],<sup>8</sup> incorporating diamagnetic Co<sup>III</sup> 3d<sup>6</sup> configurations, on the other hand, did not result in open hysteresis loops, even at 1.8 K. The ac data revealed a dominant thermally activated relaxation process ( $U_{\text{eff}} = 55 \text{ cm}^{-1}$ ) at higher temperatures (8.5–11 K), which crossed over to a frequency independent relaxation process at the lowest temperatures studied. Despite having near identical energy barriers QTM became the dominant relaxation mechanism and hence the lack of an open hysteresis loop. It was thus shown that the nature and magnitude of magnetic exchange interaction ( $J$ ) between the metal–metal center in these 3d–4f complexes helps to achieve the goal of reducing the QTM relaxation and allowing for a higher blocking temperature ( $T_{\text{B}}$ ). Moreover, it was revealed for these types of complexes that the barrier height  $U_{\text{eff}}$  can be modulated by the strength of the magnetic exchange interaction.<sup>4,9–13</sup> This was highlighted when comparing two identical metal ion topologies, [Cr<sup>III</sup>Dy<sup>III</sup>(OMe)<sub>2</sub>(O<sub>2</sub>CPh)<sub>4</sub>(mdea)<sub>2</sub>(NO<sub>3</sub>)<sub>2</sub>]<sup>7</sup> –  $J$  for Cr<sup>III</sup>–Dy<sup>III</sup> = –20.7 to –16.3 cm<sup>–1</sup> with  $U_{\text{eff}} = 54 \text{ cm}^{-1}$  and  $T_{\text{B}} = 3.7 \text{ K}$ , with [Cr<sup>III</sup>Dy<sup>III</sup>(OMe)<sub>2</sub>(acac)<sub>4</sub>(mdea)<sub>2</sub>(NO<sub>3</sub>)<sub>2</sub>] –  $J$  for Cr–Dy = –11.2 to –8.3 cm<sup>–1</sup> with  $U_{\text{eff}} = 24 \text{ cm}^{-1}$  and  $T_{\text{B}} = 1.8 \text{ K}$ .<sup>13</sup> Clearly this showed that  $U_{\text{eff}}$  and  $T_{\text{B}}$  increase as the magnetic exchange interaction increases. *Ab initio* and density functional (DFT) theoretical calculations were employed to explain these differences as well as to reveal the energetics and exchange coupling in such species. Furthermore, work on other butterfly type complexes reported by Powell *et al.* using magnetic, EPR spectral and Mössbauer effect methods, together with *ab initio* calculations, also revealed the importance of the 4f–3d magnetic exchange interaction in directing the nature of the SMM properties observed.<sup>14,15</sup>

The very first 4d–4f {Ru<sup>III</sup>Dy<sup>III</sup>} butterfly complex – [Ru<sup>III</sup>Dy<sup>III</sup>(OMe)<sub>2</sub>(O<sub>2</sub>CPh)<sub>4</sub>(mdea)<sub>2</sub>(NO<sub>3</sub>)<sub>2</sub>] (**1<sub>Dy</sub>**) was reported by our group in 2015, which displayed the same metal core and bridging arrangement as in the 3d–Dy<sup>III</sup> complexes highlighted above. **1<sub>Dy</sub>** was revealed to be the first 4d/4f heterometallic SMM.<sup>16</sup> Interestingly, upon comparison to the 3d–Dy<sup>III</sup> butterfly complexes, **1<sub>Dy</sub>** shows a significantly smaller  $U_{\text{eff}}$  value 10.7 cm<sup>–1</sup>. Theoretical studies performed by some of us in a series of {3d–4f} SMMs have shown that the key factor in enhancing the barrier height lies in inducing stronger exchange coupling and maximizing the single-ion anisotropy of the Ln<sup>III</sup> ions.<sup>9,11,17–19</sup> Due to the diffuse nature of the 4d orbitals of Ru<sup>III</sup>, a higher exchange value with Dy<sup>III</sup> ion is expected in {4d–4f} SMMs.<sup>20</sup> However, the results provided by studying **1<sub>Dy</sub>** are contrary to this hypothesis and it was found that the exchange interaction was much weaker compared to the Cr<sup>III</sup>–4f analogues. It was from this observation that a smaller  $U_{\text{eff}}$  value was rationalized, and no hysteresis was observed down to 1.8 K. The reasons as to why the magnetic exchange parameter was smaller compared to the 3d–4f analogues is an interesting question and has not been addressed.

Thus, to tackle this question and to find ways to improve  $U_{\text{eff}}$  and  $T_{\text{B}}$  values for the {Ru<sup>III</sup>Dy<sup>III</sup>} butterflies, a series of complexes has been synthesized by modifying the ligand field around the Dy<sup>III</sup> and Ru<sup>III</sup> metal ions. Two types of modifications were performed, in the first step the geometry around Dy<sup>III</sup> ion was targeted to alter the single-ion anisotropy and in the second, the carboxylate groups donor strengths were altered to improve the  $J_{\text{Ru} \dots \text{Dy}}$  exchange coupling. In this regard, we have extended the synthesis to a family of butterfly tetranuclears *viz* carboxylate-bridged [Ru<sup>III</sup>Dy<sup>III</sup>(OMe)<sub>2</sub>(O<sub>2</sub>C(4-Me-Ph)<sub>4</sub>(mdea)<sub>2</sub>(NO<sub>3</sub>)<sub>2</sub>(MeOH)<sub>4</sub>], **2<sub>Dy</sub>**, [Ru<sup>III</sup>Dy<sup>III</sup>(OMe)<sub>2</sub>(O<sub>2</sub>C(2-Cl,4,5-F-Ph)<sub>4</sub>(mdea)<sub>2</sub>(NO<sub>3</sub>)<sub>2</sub>], **3<sub>Dy</sub>**, and acac derivatives [Ru<sup>III</sup>Dy<sup>III</sup>(OMe)<sub>2</sub>(acac)<sub>4</sub>(NO<sub>3</sub>)<sub>2</sub>(edea)<sub>2</sub>], **4<sub>Dy</sub>**, where acac<sup>–</sup> = acetylacetonate, edea<sup>2–</sup> = *N*-ethyldiethanolamine dianion. To understand and quantify the mode of exchange, the Gd-analogues for complexes **1<sub>Dy</sub>** and **4<sub>Dy</sub>** have been synthesised by replacing the Dy<sup>III</sup> with Gd<sup>III</sup>; *viz*. [Ru<sup>III</sup>Gd<sup>III</sup>(OMe)<sub>2</sub>(O<sub>2</sub>CPh)<sub>4</sub>(mdea)<sub>2</sub>(NO<sub>3</sub>)<sub>2</sub>], **1<sub>Gd</sub>**, [Ru<sup>III</sup>Gd<sup>III</sup>(OMe)<sub>2</sub>(acac)<sub>4</sub>(NO<sub>3</sub>)<sub>2</sub>(edea)<sub>2</sub>], **4<sub>Gd</sub>**. The structures, magnetism and theoretical analysis of these Ru<sup>III</sup>/Ln<sup>III</sup> compounds are described. Comparisons are also made with the 3d/4f parent complex [Cr<sup>III</sup>Dy<sup>III</sup>(OMe)<sub>2</sub>(O<sub>2</sub>CPh)<sub>4</sub>(mdea)<sub>2</sub>(NO<sub>3</sub>)<sub>2</sub>]<sup>7</sup> and [Cr<sup>III</sup>Dy<sup>III</sup>(OMe)<sub>2</sub>(acac)<sub>4</sub>(mdea)<sub>2</sub>(NO<sub>3</sub>)<sub>2</sub>]<sup>12</sup> and congeners, to try and identify and explain any differences in SMM behaviour, with focus on the role of the Ru<sup>III</sup> ions.

## Experimental section

### General information

All reactions were carried out under aerobic conditions. Chemicals and solvents were obtained from commercial sources and used without further purification. Elemental analyses (CHN) were carried out by Campbell Microanalytical Laboratory, University of Otago, Dunedin, New Zealand.

**Synthesis of [Ru<sup>III</sup>Dy<sup>III</sup>(OMe)<sub>2</sub>(mdea)<sub>2</sub>(O<sub>2</sub>CPh)<sub>4</sub>(NO<sub>3</sub>)<sub>2</sub>] (**1<sub>Dy</sub>**).** RuCl<sub>3</sub>·*x*H<sub>2</sub>O (0.1 g, 0.5 mmol) and Dy(NO<sub>3</sub>)<sub>3</sub>·6H<sub>2</sub>O (0.22 g, 0.5 mmol) were dissolved in MeCN (20 mL), followed by the addition of benzoic acid (0.12 g, 1 mmol), *N*-methyldiethanolamine (0.06 mL, 0.5 mmol) and triethylamine (0.28 mL, 2.0 mmol), which resulted in a brown solution under heating. The solution was stirred for 2 hours after which time the solvent was removed to give a brown oil. This was re-dissolved in MeOH and layered with diethylether (Et<sub>2</sub>O). Within 5–7 days yellow crystals of **1<sub>Dy</sub>** had appeared, in approximate yield of 46% (crystalline product). Anal. Calculated (found) for **1<sub>Dy</sub>**: Ru<sub>2</sub>Dy<sub>2</sub>C<sub>40</sub>H<sub>48</sub>O<sub>20</sub>N<sub>4</sub>: C, 33.55 (33.71); H, 3.37 (3.47); N, 3.91 (3.99).

**Synthesis of [Ru<sup>III</sup>Dy<sup>III</sup>(OMe)<sub>2</sub>(O<sub>2</sub>C(4-Me-Ph)<sub>4</sub>(mdea)<sub>2</sub>(NO<sub>3</sub>)<sub>2</sub>(MeOH)<sub>4</sub>] (**2<sub>Dy</sub>**).** The synthesis for **1<sub>Dy</sub>** was followed except *para*-toluic acid (0.136 g, 1 mmol) was used in place of benzoic acid. Within 5–7 days yellow crystals of **2<sub>Dy</sub>** had appeared, in approximate yield of 33% (crystalline product). Anal. Calculated (found) for **2<sub>Dy</sub>**: Ru<sub>2</sub>Dy<sub>2</sub>C<sub>48</sub>H<sub>72</sub>O<sub>18</sub>N<sub>2</sub>Cl<sub>2</sub>: C, 36.88 (36.45); H, 4.64 (4.39); N, 1.97 (1.59).

**Synthesis of  $[\text{Ru}_2^{\text{III}}\text{Dy}_2^{\text{III}}(\text{OMe})_2(\text{O}_2\text{C}(2\text{-Cl},4,5\text{-F-Ph})_4(\text{mdea})_2(\text{NO}_3)_2)]$  ( $3_{\text{Dy}}$ ).** The synthesis for  $1_{\text{Dy}}$  was followed except 2-chloro-4,5-difluorobenzoic acid (0.192 g, 1 mmol) was used in place of benzoic acid. Within 5–7 days yellow crystals of  $3_{\text{Dy}}$  had appeared, in approximate yield of 33% (crystalline product). Anal. Calculated (found) for  $3_{\text{Dy}}$ :  $\text{Ru}_2\text{Dy}_2\text{C}_{40}\text{H}_{36}\text{O}_{22}\text{N}_4\text{Cl}_4\text{F}_8$ : C, 27.52 (27.29); H, 2.08 (2.11); N, 3.21 (3.34).

**Synthesis of  $[\text{Ru}_2^{\text{III}}\text{Dy}_2^{\text{III}}(\text{OMe})_2(\text{acac})_4(\text{NO}_3)_2(\text{edea})_2]$  ( $4_{\text{Dy}}$ ).** The synthesis for  $1$  was followed except *N*-ethyldiethanolamine (0.06 mL, 0.5 mmol) was used in place of *N*-methyldiethanolamine and acetylacetonone (0.1 mL, 1 mmol) was used in place of benzoic acid. Within 5–7 days yellow crystals of  $4_{\text{Dy}}$  had appeared, in approximate yield of 33% (crystalline product). Anal. Calculated (found) for  $4_{\text{Dy}}$ :  $\text{Ru}_2\text{Dy}_2\text{C}_{34}\text{H}_{60}\text{O}_{20}\text{N}_4$ : C, 29.76 (29.70); H, 4.41 (4.26); N, 4.08 (4.49).

**Synthesis of  $[\text{Ru}_2^{\text{III}}\text{Gd}_2^{\text{III}}(\text{OMe})_2(\text{mdea})_2(\text{O}_2\text{CPh})_4(\text{NO}_3)_2]$  ( $1_{\text{Gd}}$ ).** The synthesis for  $1_{\text{Dy}}$  was followed except  $\text{Gd}(\text{NO}_3)_3 \cdot 6\text{H}_2\text{O}$  (0.22 g, 0.5 mmol) was used in place of  $\text{Dy}(\text{NO}_3)_3 \cdot 6\text{H}_2\text{O}$ . Within 5–7 days yellow crystals of  $1_{\text{Gd}}$  had appeared, in approximate yield of 33% (crystalline product). Anal. Calculated (found) for  $1_{\text{Gd}}$ :  $\text{Ru}_2\text{Gd}_2\text{C}_{40}\text{H}_{48}\text{O}_{20}\text{N}_4$ : C, 33.80 (33.99); H, 3.40 (3.23); N, 3.94 (3.76).

**Synthesis of  $[\text{Ru}_2\text{Gd}_2(\text{OMe})_2(\text{acac})_4(\text{NO}_3)_2(\text{edea})_2]$  ( $4_{\text{Gd}}$ ).** The synthesis for  $4_{\text{Dy}}$  was followed except  $\text{Gd}(\text{NO}_3)_3 \cdot 6\text{H}_2\text{O}$  (0.22 g, 0.5 mmol) was used in place of  $\text{Dy}(\text{NO}_3)_3 \cdot 6\text{H}_2\text{O}$ . Within 5–7 days yellow crystals of  $4_{\text{Gd}}$  had appeared, in approximate yield of 33% (crystalline product). Anal. Calculated (found) for  $4_{\text{Gd}}$ :  $\text{Ru}_2\text{Gd}_2\text{C}_{34}\text{H}_{60}\text{O}_{20}\text{N}_4$ : C, 29.99 (30.21); H, 4.44 (4.27); N, 4.12 (4.29).

### X-ray crystallography

X-ray measurements for all complexes were performed at 150 (2) K at the Australian synchrotron MX1 beam-line. The data collection and integration were performed within Blu-Ice<sup>21</sup> and XDS<sup>22</sup> software programs. The structure was solved by direct methods (SHELXS-97), and refined (SHELXL-97) by full least matrix least-squares on all  $F^2$  data.<sup>23</sup> Crystallographic data and refinement parameters are summarized in Table S1.† Crystallographic details are available in the ESI† in CIF format. CCDC 1032631,  $1_{\text{Dy}}$ ; 2085827,  $2_{\text{Dy}}$ ; 2085828,  $3_{\text{Dy}}$ ; 2085829,  $4_{\text{Dy}}$ ; 2085830,  $1_{\text{Gd}}$ ; 2085831,  $4_{\text{Gd}}$ .†

### Magnetic measurements

The magnetic susceptibility measurements were carried out on a Quantum Design SQUID magnetometer MPMS-XL 7 operating between 1.8 and 300 K for dc-applied fields ranging from 0–5 T. Microcrystalline samples were dispersed in Vaseline in order to avoid torquing of the crystallites. The sample mulls were contained in a calibrated gelatine capsule held at the centre of a drinking straw that was fixed at the end of the sample rod. Alternating current (ac) susceptibilities were carried out under an oscillating ac field of 3.5 Oe and frequencies ranging from 0.1 to 1500 Hz.

## Results and discussion

Complexes  $1_{\text{Dy}}-4_{\text{Dy}}$  (Fig. 1 and 2) are heterometallic tetranuclear complexes consisting of two  $\text{Ru}^{\text{III}}$  and two  $\text{Dy}^{\text{III}}$  ions, with the metallic core displaying a butterfly or planar rhombus type arrangement. The  $\text{Dy}^{\text{III}}$  ions occupy the body (central) sites, with the  $\text{Ru}^{\text{III}}$  ions occupying the outer wing positions. See Table S1† for crystal space groups and experimental crystallographic details. All complexes reveal one unique  $\text{Ru}^{\text{III}}$  and  $\text{Dy}^{\text{III}}$  ion in the asymmetric unit with the symmetry related sites generated by inversion symmetry. The  $\text{Ru}^{\text{III}}$  and  $\text{Dy}^{\text{III}}$  ions are bridged *via* two  $\mu_3$  methoxide ligands, each coordinating the two  $\text{Dy}^{\text{III}}$  ions to a single  $\text{Ru}^{\text{III}}$  ion. Complexes  $1_{\text{Dy}}-4_{\text{Dy}}$  fall into two slightly different structural categories with ( $1_{\text{Dy}}-3_{\text{Dy}}$ ) displaying one structural type of butterfly with  $4_{\text{Dy}}$  displaying a modified version of the butterfly.

For complexes  $1_{\text{Dy}}-3_{\text{Dy}}$ , the core is further stabilized by two  $[\text{mdea}]^{2-}$  ligands, each of which coordinate *via* the N-atom to a  $\text{Ru}^{\text{III}}$  ion and then bridge *via* the two  $\mu_2\text{-O}$  atoms to a  $\text{Ru}^{\text{III}}$  and a  $\text{Dy}^{\text{III}}$  ion and four carboxylate ligands (benzoic acid for  $1_{\text{Dy}}$ , *para*-toluic acid for  $2_{\text{Dy}}$  and 2-chloro-4,5-fluorobenzoic acid for  $3_{\text{Dy}}$ ) each bridge a  $\text{Ru}^{\text{III}}$  to a  $\text{Dy}^{\text{III}}$  ion with the common  $\mu$  *syn-syn* bridging mode. The coordination sphere for each  $\text{Dy}^{\text{III}}$  ion

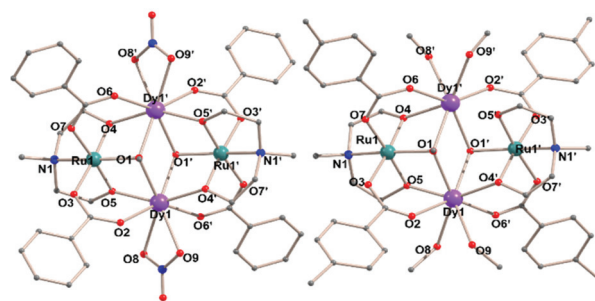


Fig. 1 Molecular structure for complexes  $1_{\text{Dy}}$  (left) and  $2_{\text{Dy}}$  (right). C atoms black, O atoms red, N atoms blue, Dy atoms purple, Ru atoms cyan.

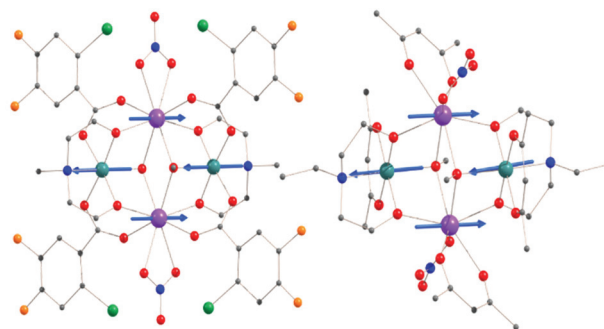


Fig. 2 Molecular structures of (left)  $3_{\text{Dy}}$  and (right)  $4_{\text{Dy}}$  along with the ground state anisotropic axis. The H atoms are omitted for clarity. Colour scheme;  $\text{Ru}^{\text{III}}$ , pale green;  $\text{Dy}^{\text{III}}$ , purple; O red; N blue; C light grey; Cl green; F orange. The blue arrows represent the alignment of ground state anisotropy axes for each metal center.

is completed for  $1_{\text{Dy}}$  and  $3_{\text{Dy}}$  by a single chelating nitrate ligand, while for complex  $2_{\text{Dy}}$ , two MeOH are coordinated to each  $\text{Dy}^{\text{III}}$ . The  $\text{Ru}^{\text{III}}$  ions are six-coordinate with distorted octahedral geometries, with a deviation of 0.385, 0.518 and 0.433 from ideal octahedron for  $1_{\text{Dy}}-3_{\text{Dy}}$  respectively, from continuous SHAPE<sup>24</sup> measurement and ChMS analysis.<sup>25</sup> The average  $\text{Ru}-\text{L}_{\text{N,O}}$  bond distance is 2.04 Å, 2.04 Å and 2.07 Å for  $1_{\text{Dy}}-3_{\text{Dy}}$ , respectively. The  $\text{Dy}^{\text{III}}$  ions are both eight-coordinate and display distorted square-antiprismatic (SAP) geometries with a deviation of 1.637, 0.845 and 1.725 from the ideal square antiprism for  $1_{\text{Dy}}-3_{\text{Dy}}$ , respectively. The average  $\text{Dy}-\text{O}$  bond length is 2.36 Å, 2.35 Å and 2.48 Å, for  $1_{\text{Dy}}-3_{\text{Dy}}$ , respectively. Selected bond lengths and angles are given in Tables S2b and c.† We note that complexes  $1_{\text{Dy}}-3_{\text{Dy}}$  are analogous to the earlier reported 3d-4f butterflies when using a carboxylate co-ligand, showing an identical metal ion topology and first coordination sphere for all bridging ligands.<sup>7</sup>

For complex  $4_{\text{Dy}}$  the ligand  $(\text{acac})^-$  is used in place of a carboxylate ligand and *N*-ethyldiethanolamine used as the amine-polyalcohol. The complex is stabilized around the periphery by two amine-polyalcohol ligands which coordinate *via* the N-atom to the  $\text{Ru}^{\text{III}}$  ions and then bridge the  $\text{Ru}^{\text{III}}$  to the  $\text{Dy}^{\text{III}}$  ions *via* two  $\mu_2$  O-atoms. The coordination sphere of each  $\text{Ru}^{\text{III}}$  ion are completed with one chelating  $(\text{acac})^-$  ligand, while a single chelating  $(\text{acac})^-$  and a nitrate ligand complete the coordination environment of the  $\text{Ru}^{\text{III}}$  ions. This results in six coordinate  $\text{Ru}^{\text{III}}$  ions with distorted octahedral geometries, with a deviation of 1.306 from an ideal octahedron. The average  $\text{Ru}-\text{L}_{\text{N,O}}$  bond distance is 2.03 Å. The  $\text{Dy}^{\text{III}}$  ions are all eight coordinate with distorted square antiprismatic geometries, with a deviation of 1.306 from ideal SAP geometry. The average  $\text{Dy}-\text{O}$  bond length is 2.38 Å (see Table S2d† for selected bond lengths).

Structural comparisons of  $4_{\text{Dy}}$  to  $1_{\text{Dy}}-3_{\text{Dy}}$  reveal the absence of a carboxylate bridging pathway between the  $\text{Dy}^{\text{III}}$  and  $\text{Ru}^{\text{III}}$  ions, with two chelating ligands found at the  $\text{Dy}^{\text{III}}$  sites, opposed to one ligand observed for  $1_{\text{Dy}}$  and  $3_{\text{Dy}}$ . A single chelating  $(\text{acac})^-$  is also found at the  $\text{Ru}^{\text{III}}$  sites, not seen for  $1_{\text{Dy}}-3_{\text{Dy}}$ .

The  $\text{Gd}^{\text{III}}$  analogues  $1_{\text{Gd}}$  and  $4_{\text{Gd}}$  are isostructural with the  $\text{Dy}^{\text{III}}$  parents  $1_{\text{Dy}}$  and  $4_{\text{Dy}}$ , respectively. The average bond length between  $\text{Gd}-\text{O}$  is found to be 2.39 Å and 2.38 Å for complex  $1_{\text{Gd}}$  and  $4_{\text{Gd}}$  respectively (see Tables S2a and S2e† for selected bond lengths).

### Magnetic studies

Direct current magnetic susceptibility measurements on polycrystalline samples of the  $\text{Dy}^{\text{III}}$  analogues, complexes  $2_{\text{Dy}}-4_{\text{Dy}}$  and  $\text{Gd}^{\text{III}}$  analogues  $1_{\text{Gd}}$ ,  $4_{\text{Gd}}$  have been performed over the temperature range 2–300 K in dc fields of 0.1 T and 1.0 T. The  $\chi_{\text{M}}T$  vs.  $T$  plots are shown in Fig. 3 and Fig. S2.† Magnetic data for  $1_{\text{Dy}}$  which have previously been reported are also shown (Fig. S2†).<sup>16</sup> The molar magnetic susceptibility times temperature ( $\chi_{\text{M}}T$ ) value of 28.83, 29.12 and 29.96  $\text{cm}^3 \text{K mol}^{-1}$  for  $2_{\text{Dy}}-4_{\text{Dy}}$ , respectively, at 300 K, are in good agreement with the calculated value ( $(2 \times 14.17) + (2 \times 0.37) = 29.08 \text{ cm}^3 \text{K mol}^{-1}$ )

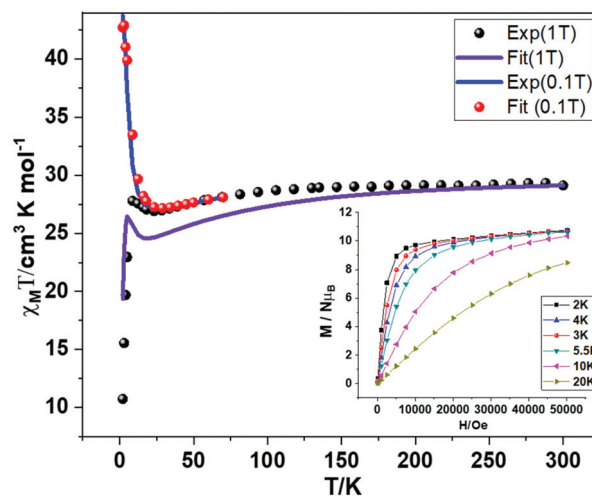


Fig. 3  $\chi_{\text{M}}T$  vs.  $T$  for complex  $3_{\text{Dy}}$  with an applied magnetic field of 1 T and 0.1 T. The observed and fitted plots are shown. The inset represents the  $M$  vs.  $H$  plot at different temperatures. See ESI Fig. S2† for the observed and fitted data for the other complexes.

of two  $\text{Dy}^{\text{III}}$  ( $S = 5/2$ ,  $L = 5$ ,  ${}^6\text{H}_{15/2}$ ,  $g = 4/3$ ,  $C = 14.17 \text{ cm}^3 \text{K mol}^{-1}$ ) and two  $\text{Ru}^{\text{III}}$  ( $S = \frac{1}{2}$ ,  $g = 2.0$ ,  $C = 0.37 \text{ cm}^3 \text{K mol}^{-1}$ ) non-interacting centers. In the field 1 T, as the temperature is decreased the  $\chi_{\text{M}}T$  product decreases gradually down to 25 K, below which an upturn is observed for  $2_{\text{Dy}}$  and  $3_{\text{Dy}}$ , while the  $\chi_{\text{M}}T$  product plateaus for  $4_{\text{Dy}}$ . The slight difference in the profile is likely due to structural differences and the different bridging pathways between ( $2_{\text{Dy}}$  and  $3_{\text{Dy}}$ ) and  $4_{\text{Dy}}$ , resulting in differing magnetic exchange interactions. At 0.1 T at the lowest temperatures a large upturn in  $\chi_{\text{M}}T$  is observed for  $2_{\text{Dy}}-4_{\text{Dy}}$ . The low temperature behaviour is field dependent, owing to the Zeeman splitting of the ground multiplet. The high temperature decrease (300–25 K) can be attributed to the depopulation of the excited  $m_l$  states of the  $\text{Dy}^{\text{III}}$  ions, while the increase at lower temperatures suggests non-negligible exchange interactions between the  $\text{Ru}^{\text{III}}$  and the  $\text{Dy}^{\text{III}}$  ions (see *ab initio* and DFT analysis below). The isothermal magnetization ( $M$ ) measurements, plotted as a function of the magnetic field ( $H$ ), each display a rapid increase in magnetization below 2 T, before following a more gradual linear-like increase, without saturating (Fig. 3 (inset) and Fig. S3†). This, along with the field dependence observed in the magnetic susceptibility plot suggests a significant magnetic anisotropy is present.

The direct current magnetic susceptibility measurements on polycrystalline samples of the  $\text{Gd}^{\text{III}}$  analogues, complexes  $1_{\text{Gd}}$  and  $4_{\text{Gd}}$  have also been performed over the temperature range 2–300 K in dc fields of 0.1 T and 1.0 T and are shown in Fig. S3.† These measurements were performed to help gauge the strength of the magnetic exchange interaction by fitting the experimental data using the PHI program.<sup>26</sup> The results of which are discussed later (Fig. S2† for the fits of the experimental data).

In order to probe for any slow magnetic relaxation for the  $\{\text{Ru}_2^{\text{III}}\text{Dy}_2^{\text{III}}\}$  complexes variable temperature and variable fre-

frequency alternating current (ac) susceptibility measurements were performed with an oscillating ac field of 3.5 Oe under a zero applied dc field. These measurements revealed clear frequency and temperature dependent maxima (1.8–5 K) in the out-of-phase ( $\chi''_M$ ) (Fig. 4) component for complexes  $1_{Dy}$  and  $3_{Dy}$ , signifying SMM behavior. For  $2_{Dy}$  and  $4_{Dy}$  tails of peaks are only found at the lowest temperatures measured (1.8 K) signifying probable SMM behaviour. To fully characterize these complexes, lower temperatures are required (Fig. S4†). Thus, we find  $1_{Dy}$  and  $3_{Dy}$  display slow magnetic relaxation at higher temperatures compared to  $2_{Dy}$  and  $4_{Dy}$  and can be considered better SMMs. An analysis of the relaxation data for  $1_{Dy}$  has previously been reported, with a  $U_{eff}$  parameter of  $10.4 \text{ cm}^{-1}$ .<sup>16</sup> Plots of  $\chi''_M$  vs. frequency and  $\chi''_M$  vs.  $\chi'_M$  are shown in Fig. 4 for both  $1_{Dy}$  (top) and  $3_{Dy}$  (bottom). The Cole–Cole plots reveal semicircular profiles confirming a single relaxation process (Fig. 4, right inset). Using CC-FIT<sup>27</sup> the temperature dependent relaxation data for  $3_{Dy}$  were used to extract the relaxation times including all the possible relaxation processes (Fig. 4, right). The following equation [ $1/\tau = 1/\tau_{QTM} + CT^n + \tau_0^{-1} \exp(U_{eff}/k_B T)$ ] was used, where  $1/\tau_{QTM}$  corresponds to the relaxation process

via a quantum tunneling pathway, the  $CT^n$  term corresponds to the relaxation occurring via a Raman process, and the last term accounts for the Orbach relaxation pathway.<sup>28,29</sup> As the previously reported  $U_{eff}$  value for  $1_{Dy}$  was extracted considering only a Orbach processes, we also fitted the data for  $1_{Dy}$  using the equation above including all relaxation processes for comparison. The values obtained from the best fit are  $n = 6.3 \pm 0.1$ ,  $C = 1.0 \pm 0.1 \text{ s}^{-1} \text{ K}^{-6}$ ,  $U_{eff} = 41 \pm 1 \text{ K}$  ( $28 \text{ cm}^{-1}$ ) and  $\tau_0 = 1.01 \pm 0.02 \times 10^{-11} \text{ s}$  for  $1_{Dy}$  and  $n = 6.0 \pm 0.2$ ,  $C = 0.9 \pm 0.1 \text{ s}^{-1} \text{ K}^{-6}$ ,  $U_{eff} = 45 \pm 2 \text{ K}$  ( $31 \text{ cm}^{-1}$ ) and  $\tau_0 = 1.01 \pm 0.02 \times 10^{-10} \text{ s}$  for  $3_{Dy}$ . A QTM relaxation time,  $\tau_{QTM}$ , of 0.006 s for  $1_{Dy}$  and 0.04 s for  $3_{Dy}$  was estimated. The  $U_{eff}$  of complex  $1_{Dy}$  from the above equation is higher than the reported  $U_{eff}$  value ( $\sim 10 \text{ cm}^{-1}$ ) of  $1_{Dy}$ .<sup>16</sup> The change in  $U_{eff}$  of complex 1 is mainly because of considering all the relaxation parameters here, instead of simply considering an Orbach processes. This reveals the importance of considering all relaxation mechanisms when performing an analysis on relaxation data. While the out-of-phase signals are only beginning to appear at temperatures down to 1.8 K for  $2_{Dy}$  and  $4_{Dy}$  under a zero dc field, we do observe out-of-phase susceptibility maxima for  $2_{Dy}$  and  $4_{Dy}$ , in

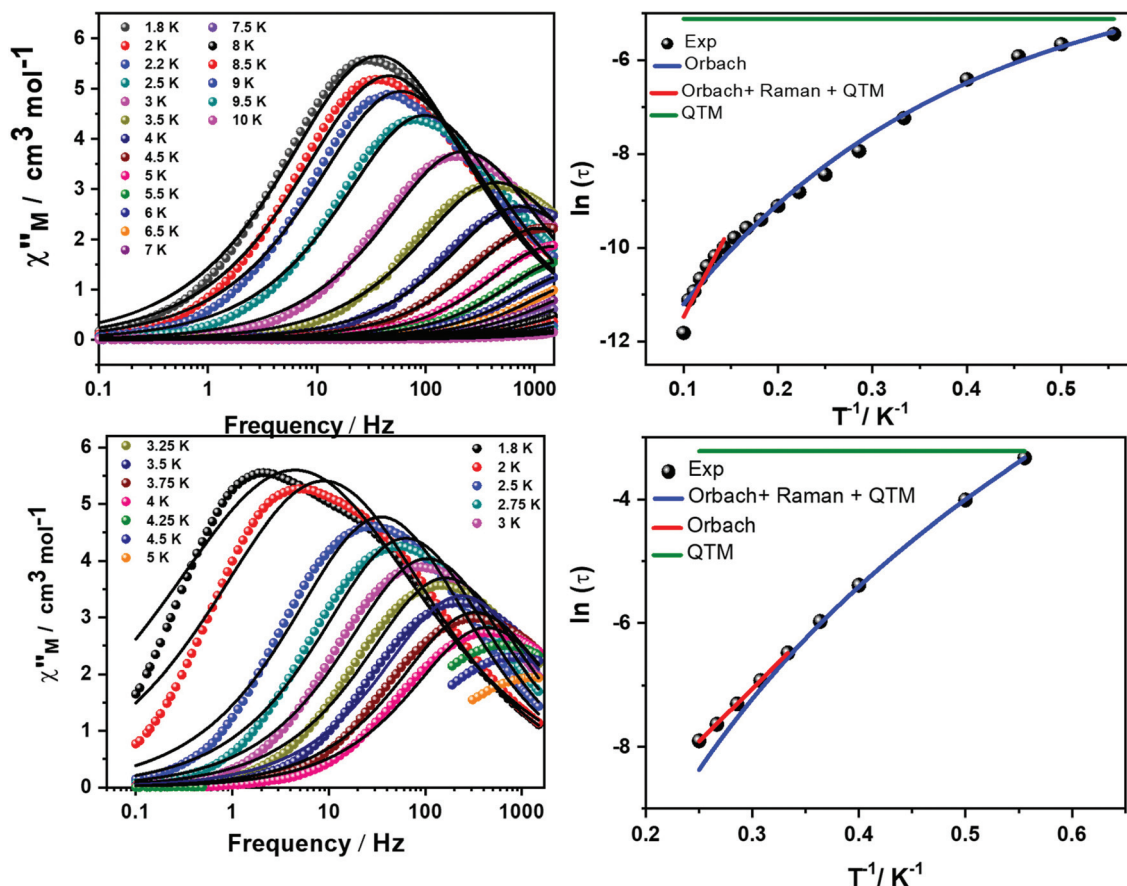


Fig. 4  $\chi''_M$  vs. frequency plots for  $1_{Dy}$  (top-left) and  $3_{Dy}$  (bottom-left), at  $H_{dc} = 0$  Oe. Magnetization relaxation time ( $\tau$ ), plotted as  $\ln(\tau)$  versus  $T^{-1}$  for  $1_{Dy}$  (top right)  $3_{Dy}$  (bottom-right). The solid red line corresponds to fitting of the Orbach relaxation process and the solid blue line represents the best fitting to the multiple relaxation process. The horizontal green line represents the QTM relaxation time. Cole–Cole plots between 1.8–5 K are given in ESI Fig. S4.† The solid black lines are fitted values obtained from CC-fit program using the parameters given in the text.<sup>27,30</sup>

the presence of a static dc field (500 Oe and 2000 Oe) (Fig. S4†), the reason for which is likely due to quenching of QTM relaxation processes, commonly found in Ln<sup>III</sup> based SMMs. For the {Ru<sup>III</sup>Gd<sup>III</sup>} analogues no signal was observed in a zero applied dc field – however for **4**<sub>Gd</sub> we observe out-of-phase tails at 2000 Oe (Fig. S4†). This is likely due to the presence of the anisotropic Ru<sup>III</sup> ion.

### Computational studies

To gain insight into the magnetic relaxation dynamics originating from the constituent single paramagnetic centers as well as from the exchanged-coupled states and how the nature of exchange coupling is playing a role, *ab initio* and density functional (DFT) calculations have been performed utilising the crystal structure of each complex. *Ab initio* calculations have been performed using the MOLCAS 8.0 package,<sup>31</sup> where CASSCF/RASSI-SO/SINGLE\_ANISO/POLY\_ANISO methodologies have been employed.<sup>32,33,34–36</sup> DFT calculations were performed using the G16 package.<sup>37</sup> For the SINGLE\_ANISO module, magnetic properties on individual centers have been calculated by replacing each metal ion with a diamagnetic one (Lu<sup>III</sup> for Dy<sup>III</sup> and Y<sup>III</sup> for Ru<sup>III</sup>). For the Gaussian BS-DFT calculations,<sup>38,39</sup> calculations were performed on the X-ray obtained geometry by replacing Dy<sup>III</sup> with Gd<sup>III</sup> for complexes **1**<sub>Dy</sub>–**4**<sub>Dy</sub> and as well as the Gd<sup>III</sup> analogue complexes **1**<sub>Gd</sub> and **4**<sub>Gd</sub>. The details of functional and basis sets are provided in Table S3 of the ESI.† To calculate exchange for complex **1**<sub>Gd</sub>–**4**<sub>Gd</sub>, the values obtained with Gd have been rescaled by multiplying 5/7 for five unpaired electrons of Dy<sup>III</sup>.

For the individual paramagnetic centers for complexes **1**<sub>Dy</sub>–**4**<sub>Dy</sub>, the energies of low-lying Kramers doublets (KDs) are provided in Table 1 along with the ground state  $g_{zz}$  anisotropy. Due to the unquenched orbital moment of the 4d ( $t_{2g}^5$ ) ion, the Ru<sup>III</sup> is also expected to exhibit anisotropy. The <sup>2</sup>T<sub>2g</sub> doublet ground state is arising due to a large crystal field splitting by the 4d orbitals in Ru<sup>III</sup> centers.<sup>20</sup> The Dy<sup>III</sup> ion is found to have highly axial anisotropy, whereas the Ru<sup>III</sup> ion has a rhombic set of g-tensors, which is expected to influence the SMM characteristics. The computed crystal field pattern for the Dy<sup>III</sup> ion is found to vary among **1**<sub>Dy</sub> to **4**<sub>Dy</sub>, with the largest ground to first excited state gap noted for **3**<sub>Dy</sub> followed by **1**<sub>Dy</sub>. If we compare (**1**<sub>Dy</sub> and **3**<sub>Dy</sub>) vs. **2**<sub>Dy</sub>, the chelating nitrate group coordinated to the Dy<sup>III</sup> ion in (**1**<sub>Dy</sub> and **3**<sub>Dy</sub>) is replaced by two MeOH ligands in **2**<sub>Dy</sub>. This alteration decreases the overall crystal field of the eight low lying.

KDs, and **2**<sub>Dy</sub> has the smallest energy gap among all complexes studied. This is due to the relatively smaller negative charge exhibited by the methanolic oxygen atoms compared to nitrate groups and reflected in the computed LoProp charges (Fig. S5†).<sup>40</sup> Furthermore, the first excited KD of **2**<sub>Dy</sub> is found to have a significant transverse component due to this alteration in geometry ( $g_{xx} = 0.614$ ,  $g_{yy} = 0.785$ ,  $g_{zz} = 16.169$  for **2**<sub>Dy</sub>, compared to  $g_{xx} = 0.010$ ,  $g_{yy} = 0.015$ ,  $g_{zz} = 16.886$  for **3**<sub>Dy</sub>). This large transverse anisotropy at the first excited state reveals that

**Table 1** Low lying KDs for the Dy<sup>III</sup> and Ru<sup>III</sup> centers for complex **1**<sub>Dy</sub>–**4**<sub>Dy</sub> along with the ground state  $g$ -tensor values. See ref. 16 for **1**<sub>Dy</sub> and **1**-Ru

Complexes	<b>1</b> -Dy	<b>1</b> -Ru	<b>2</b> -Dy	<b>2</b> -Ru
KD1	0.0	0	0.0	0
KD2	179	3972	166.6	4034.9
KD3	278	5115	221.9	5260.5
KD4	306	15 188	265.3	15 082.3
KD5	319	15 260	290.6	15 319.6
KD6	379	15 411	371.0	15 608.9
KD7	423	15 607	410.6	15 855.6
KD8	546	17 874	450.3	17 784.1
$g_{xx}$	0.0051	2.65	0.0013	2.6430
$g_{yy}$	0.0052	2.48	0.0020	2.4760
$g_{zz}$	19.74	1.54	19.8591	1.5565
Complexes	<b>3</b> -Dy	<b>3</b> -Ru	<b>4</b> -Dy	<b>4</b> -Ru
KD1	0.0	0.0	0.0	0.0
KD2	188.7	4165.7	162.1	3554.3
KD3	265.7	5398.4	292.2	4519.3
KD4	326.6	13 324.3	318.9	16 969.7
KD5	363.2	13 461.4	399.3	17 146.3
KD6	409.6	20 492.0	524.1	19 314.0
KD7	458.6	20 600.9	636.7	19 609.3
KD8	565.6	20 652.5	910.9	19 724.2
$g_{xx}$	0.0022	2.6283	0.0114	2.6551
$g_{yy}$	0.0035	2.4168	0.0186	2.5584
$g_{zz}$	19.7809	1.5727	19.8596	1.4656

the  $m_j = \pm 13/2$  state is significantly influenced due to the substitution while the ground state is barely affected. From the single-ion perspective, this transverse anisotropy precludes the zero field SMM behavior for complex **2**<sub>Dy</sub>. Comparing the single ion anisotropy between complexes **3**<sub>Dy</sub> and **4**<sub>Dy</sub>, the latter lacks the bridging carboxylate between the Dy<sup>III</sup> and Ru<sup>III</sup> ions, thus showing a transverse anisotropy in the first excited state ( $g_{xx} = 0.310$ ,  $g_{yy} = 0.795$ ,  $g_{zz} = 16.383$ ). From the single ion perspective it is expected that among the three complexes, **3**<sub>Dy</sub> should be the best SMM followed by complex **4**<sub>Dy</sub> and then **2**<sub>Dy</sub> (Fig. 5). Comparing **3**<sub>Dy</sub> to the reported complex **1**<sub>Dy</sub>, it is clear that electron withdrawing substituents like Cl/F on the benzoate ring have improved the single ion properties by changing the local charge on the ligands coordinated to the metal ion. It is also clear comparing **3**<sub>Dy</sub> to **2**<sub>Dy</sub> that by replacing the chelating (NO<sub>3</sub>)<sup>-</sup> ligand on the Dy<sup>III</sup> ion with MeOH reduces the size of the anisotropy barrier, again due to ligand charge reasons (see LoProp charges, Fig. S5†), reducing the effectiveness of the SMM (Fig. 5). However, as the exchange coupling is expected to be significant (*vide infra*), it is expected that the overall magnetic dynamics of the complexes arise from the exchange-coupled state of the whole molecule. Thus, a combination of the single ion properties along with the exchange coupled state determines the overall magnetic relaxation, which is explored below.

We now discuss the effects the magnetic exchange interactions have on the SMM properties. Perusal of the tetranuc-

Table 2 Exchange coupling values in  $\text{cm}^{-1}$  estimated using *ab initio* and DFT calculations for the complexes

Complexes	Lines model			DFT		
	$J_{\text{Ln-Ru}}$ ( $J'_{\text{Ln-Ru}}$ )	$J_{\text{Ln-Ln}}$	$J_{\text{Ru-Ru}}$	$J_{\text{Ln-Ru}}$ ( $J'_{\text{Ln-Ru}}$ )	$J_{\text{Ln-Ln}}$	$J_{\text{Ru-Ru}}$
$1_{\text{Dy}}$	-2.35 (-1.45)	0.003	-0.05	-2.3 (-1.5)	0.003	-0.05
$1_{\text{Gd}}^a$	-2.20 (-2.00)	0.01	-0.07	-2.12 (-1.98)	0.01	-0.07
$2_{\text{Dy}}$	-2.35 (-1.50)	0.01	-0.04	-2.3 (-1.6)	0.01	-0.04
$3_{\text{Dy}}$	-2.42 (-2.25)	0.01	-0.07	-2.4 (-2.3)	0.01	-0.07
$4_{\text{Dy}}$	-1.9 (-1.5)	0.02	-0.03	-1.8 (-1.4)	0.02	-0.03
$4_{\text{Gd}}^a$	-2.30-2.10	0.02	-0.05	-2.26 (-1.80)	0.02	-0.04

<sup>a</sup> Isotropic exchange coupling here was fitted using PHI software.<sup>26</sup>

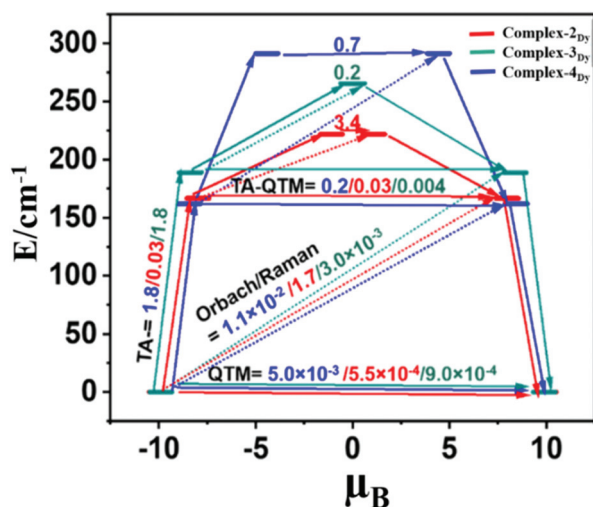


Fig. 5 Mechanism of magnetic relaxation computed for the individual  $\text{Dy}^{\text{III}}$  centers for complexes  $2_{\text{Dy}}-4_{\text{Dy}}$ , where energy is plotted against the function of the magnetic moment. Numbers on the respective arrows represent the transition probability between the corresponding states joined by the arrows.

lear metal ion topology reveals that there are at least four different exchange coupling interactions present in each complex (i) two  $J_{\text{Ru}\dots\text{Dy}}$  exchange pathways as the Ru–O–Dy angles falls into two categories as per the symmetry present (average angle of 95.4 vs. 96.6 in  $1_{\text{Dy}}$ ) (ii) one  $J_{\text{Dy}\dots\text{Dy}}$  exchange interaction and (iii) one  $J_{\text{Ru}\dots\text{Ru}}$  exchange coupling. As the number of exchange interactions are relatively large, to reduce the number of interactions, we have employed the  $\text{Gd}^{\text{III}}$  analogues where isotropic exchange coupling can be estimated directly using DFT techniques.<sup>41,42</sup> DFT calculations performed on  $1_{\text{Gd}}$ , and  $4_{\text{Gd}}$  geometries yield  $J_{\text{Gd}\dots\text{Ru}}$  exchange coupling value of  $-2.12 \text{ cm}^{-1}$  and  $-2.26 \text{ cm}^{-1}$ , respectively. The  $J_{\text{Gd}\dots\text{Gd}}$  exchange is estimated to be  $0.01 \text{ cm}^{-1}$  and  $0.02 \text{ cm}^{-1}$ , while  $J_{\text{Ru}\dots\text{Ru}}$  is estimated to be weakly antiferromagnetic in both cases ( $-0.07$  and  $-0.04 \text{ cm}^{-1}$ ) (see Table 2 for all calculated exchange values). This set of exchange parameters yield a ground state of  $S = 6$  for  $1_{\text{Gd}}$  and  $4_{\text{Gd}}$  with a spin on  $\text{Ru}^{\text{III}}$  centers oriented “down” and spin on  $\text{Gd}^{\text{III}}$  centers orientated “up”. The estimated values as well as the ground state, are consistent with the experimental results obtained

from fitting (see Table 2). The computed spin density plot for  $1_{\text{Dy}}/1_{\text{Gd}}$  is shown in Fig. 7. The unpaired electron in  $\text{Ru}^{\text{III}}$  is found in a  $\delta$ -type  $d_{xy}$  orbital, which is found to promote strong spin delocalization as the bridging oxygen atoms gain significant spin densities. The  $\text{Gd}^{\text{III}}$  center, on the other hand, promotes spin polarization. One of the bridging oxygen atoms in the bis- $\mu$ -alkoxo bridge connecting the  $\text{Ru}^{\text{III}}$  and  $\text{Gd}^{\text{III}}$  ion was found to have significant spin density, which opens up a super-exchange pathway with a  $\text{Gd}^{\text{III}}$  4f orbital. Additionally, the carboxylate bridge’s oxygen atoms connected to the  $\text{Ru}^{\text{III}}$  ion also have significant spin density due to spin delocalization. This also opens up additional  $d_{xy}$ -4f overlaps that contributes to the antiferromagnetic part of the exchange interaction. The ferromagnetic contribution to the  $\{4d-4f\}$  exchange, on the other hand, arises from charge transfer from the  $\text{Ru}^{\text{III}}$  4d orbital to the  $\text{Gd}^{\text{III}}$  5d orbital and is expected to be weak due to the  $\delta$ -type  $d_{xy}$  orbital on the  $\text{Ru}^{\text{III}}$  center. A weak ferromagnetic contribution coupled with stronger 4d–4f overlap leads to a relatively large antiferromagnetic coupling. While the strength of coupling was found to vary across the series, the sign of which remains the same in all studied complexes. The  $\text{Gd}^{\text{III}}-\text{O}-\text{Gd}^{\text{III}}$  angle is found to in the range of 112 to 114° and is expected to be ferromagnetic as per the correlation established earlier.<sup>37</sup> In addition to this, even the small variation observed in  $J_{\text{Gd}\dots\text{Gd}}$  is found to correlate to the angle such that lower angles yield less ferromagnetic exchange and a larger angle yield larger ferromagnetic coupling.<sup>43</sup> The  $J_{\text{Ru}\dots\text{Ru}}$  exchange pathway is a next-nearest-neighbor interaction (1,3 interaction) which is estimated to be antiferromagnetic in nature as the  $\text{Ru}^{\text{III}}$   $d_{xy}$  orbital are diffused and are likely to interact *via* the  $\text{Ln}^{\text{III}}$  ions as shown in several earlier examples.<sup>42</sup> Magnetostructural correlation developed for such 1,3 interactions mediated *via*  $\text{Gd}^{\text{III}}$  ions reveals a parabolic feature with Ru–Gd–Ru angles less than 120° yielding antiferromagnetic coupling with lower angles enhancing the strength. Here for  $1_{\text{Gd}}$  and  $4_{\text{Gd}}$ , the Ru–Gd–Ru angles are 104.5° and 105.0°, respectively, and the estimated sign and the strength of  $J_s$  (see Table 2) match well with the correlation previously developed.<sup>18,44</sup>

To estimate the magnetic coupling for the  $\text{Dy}^{\text{III}}$  analogues, we rely on the Lines model<sup>45</sup> and take the exchange information from the corresponding  $\text{Gd}^{\text{III}}$  complexes to understand the relative sign and strength of the  $J_s$  expected. The Lines

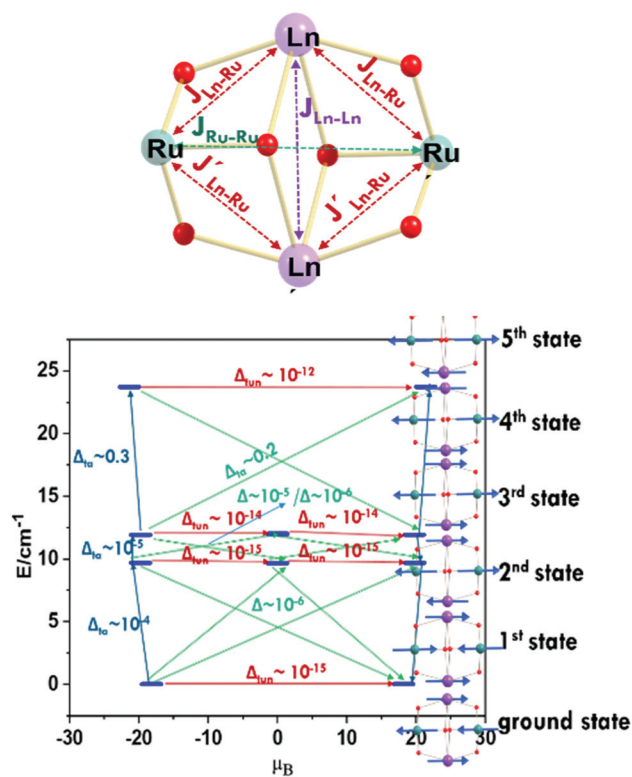


Fig. 6 Mode of exchange coupling between the metal–metal centers (top). Magnetic relaxation dynamics were obtained from Polyaniso fitting for complex  $3_{\text{Dy}}$  (bottom).

approach adapt the following Hamiltonian using the coupling scheme in Fig. 6,

$$\hat{H}_{\text{exch}} = -J_{\text{Ru1-Ru2}}\hat{S}_{\text{Ru1}}\hat{S}_{\text{Ru2}} - J_{\text{Dy1-Dy2}}\hat{S}_{\text{Dy1}}\hat{S}_{\text{Dy2}} \\ - 2[J_{\text{Dy1-Ru1}}\hat{S}_{\text{Dy1}}\hat{S}_{\text{Ru1}}] - 2[J_{\text{Dy2-Ru2}}\hat{S}_{\text{Dy2}}\hat{S}_{\text{Ru2}}]$$

The  $J$  values estimated using the Lines model are given in Table 2, and the computed values are also consistent with the DFT estimates (obtained using appropriate scaling for the  $\text{Dy}^{\text{III}}$  ion, see computational details). The average  $J_{\text{Ru}\dots\text{Dy}}$  values follow the trend  $3_{\text{Dy}} > 1_{\text{Dy}} > 2_{\text{Dy}} > 4_{\text{Dy}}$ , and this value also correlates well with the antiferromagnetic {3d–4f} coupling proposed earlier for  $\{\text{Cr}^{\text{III}}\dots\text{Gd}^{\text{III}}\}$  interactions, with smaller angles yielding stronger antiferromagnetic coupling.<sup>39</sup> The average Ru–O–Dy angle is found to be smallest in complex  $3_{\text{Dy}}$  ( $95.8^\circ$ ), while it is found to be largest in  $4_{\text{Dy}}$  ( $96.6^\circ$ ).  $J_{\text{Ru}\dots\text{Dy}}$  is found to be significantly small for  $4_{\text{Dy}}$ , and this is due to the absence of the carboxylate bridge connecting the  $\text{Dy}^{\text{III}}$  and  $\text{Ru}^{\text{III}}$  ions, which is found to offer an additional exchange pathway (see Fig. 7 for spin density plot) and hence a stronger antiferromagnetic coupling for other complexes. The order of spin density on the bridging carboxylate is found to be in the order of  $3_{\text{Dy}} > 1_{\text{Dy}} > 2_{\text{Dy}} > 4_{\text{Dy}}$  which reflects in the estimated  $J_{\text{Ru}\dots\text{Dy}}$  exchange values. The absence of bridging carboxylate pathways in complex  $4_{\text{Dy}}$ , reduces the exchange by up to 25% compared to that in  $3_{\text{Dy}}$  which reflects from the spin density plot.

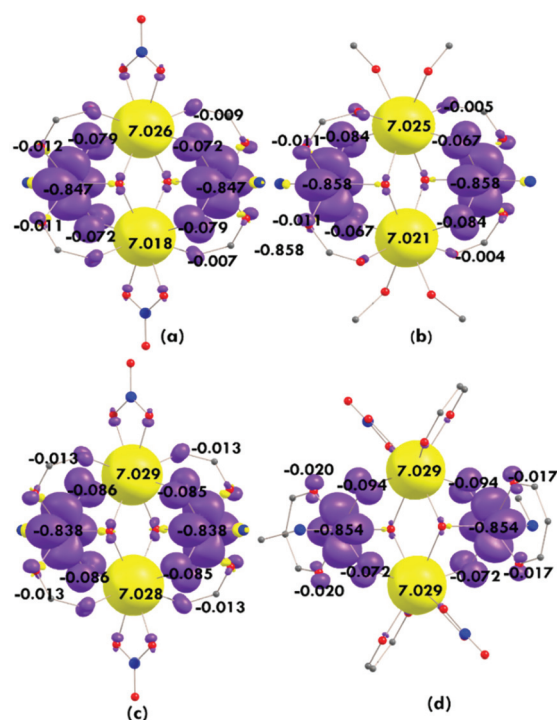


Fig. 7 Spin density plot for the broken symmetry state for complex  $1_{\text{Dy}}$  (a),  $2_{\text{Dy}}$  (b),  $3_{\text{Dy}}$  (c) and  $4_{\text{Dy}}$  (d) calculated by replacing the  $\text{Dy}^{\text{III}}$  by  $\text{Gd}^{\text{III}}$ . Yellow lobe represents the alpha and violet lobe represents the beta electron density.

It is important to note here that the  $J_{\text{Ru}\dots\text{Dy}/\text{Gd}}$  is smaller than  $J_{\text{Cr}\dots\text{Dy}/\text{Gd}}$  found earlier,<sup>7,13</sup> and this is due to the fact the  $\delta_{xy}$  orbital, which hosts the unpaired electron in  $\text{Ru}^{\text{III}}$  overlap with the 4f orbital *via* one of the  $\mu$ -alkoxo bridge. However,  $\text{Cr}^{\text{III}}$  has a  $t_{2g}^3$  electronic configuration, which leads to efficient overlap of these orbitals with 4f orbitals of  $\text{Ln}^{\text{III}}$  ion resulting in a stronger antiferromagnetic coupling.

To avoid overparameterization in the Lines model,<sup>45</sup> the  $J_{\text{Dy}\dots\text{Dy}}$  and  $J_{\text{Ru}\dots\text{Ru}}$  values are fixed as per the DFT estimates (see Table 2). The POLY\_ANISO<sup>46,47</sup> developed mechanism of magnetization relaxation that takes into account all the exchange coupling values are shown in Fig. 6 and Fig. S7.† The  $g_{zz}$  axis of the  $\text{Dy}^{\text{III}}$  ion in the exchange-coupled ground state was found to be collinear with respect to each other, while the  $\text{Ru}^{\text{III}}$  spins are flipped due to dominant antiferromagnetic coupling (Fig. 2 and 6). This strong coupling quenches the tunneling as the  $\Delta_{\text{tun}}$  is computed to be negligible, offering zero-field SMM behavior for  $3_{\text{Dy}}$ . Additionally, the Orbach/Raman process to other spin-flipped excited states is also smaller allowing the relaxation to proceed *via* higher excited states. Although a group of excited states lies around  $\sim 10 \text{ cm}^{-1}$ , the  $\Delta_{\text{tun}}$  values are still lower with the relaxation expected to take place *via* 5<sup>th</sup> excited states that sets the  $U_{\text{cal}}$  value to 33 K, which matches with the experimental data ( $U_{\text{eff}} = 45 \text{ K}$ ). For complexes,  $2_{\text{Dy}}$  and  $4_{\text{Dy}}$ , on the other hand, one of the estimated ( $J_{\text{Ru-Dy}}$ ) is weak and does not offer stronger quenching

similar to the one seen in  $3_{\text{Dy}}$ . Hence, the  $\Delta_{\text{tun}}$  values, as well as the Orbach/Raman relaxation to higher excited multiplets, are relatively larger. The excited states also lie much closer, suggesting very weak zero-field SMM behavior, as seen in experiments.

Finally we note that Long *et al.* have just reported a {4d-4f} trinuclear  $\text{Mo}^{\text{V}}\text{S}_4^{3-}$ -bridged family  $[\text{Co}(\text{C}_5\text{Me}_5)_2][(\text{C}_5\text{Me}_5)_2\text{Ln}(\mu\text{-S})_2\text{Mo}(\mu\text{-S})_2\text{Ln}(\text{C}_5\text{Me}_5)_2]$  ( $\text{Ln} = \text{Y}, \text{Gd}, \text{Tb}, \text{Dy}$ ), in which the  $\text{Gd}^{\text{III}}$  example show large ferromagnetic coupling between the  $S = 7/2$ ,  $S = 1/2$ ,  $S = 7/2$  centres of  $J = +16.1$  (2)  $\text{cm}^{-1}$ , while the  $\text{Dy}^{\text{III}}$  derivative showed a  $U_{\text{eff}} = 68$   $\text{cm}^{-1}$ .<sup>48</sup> The work detailed here and by Long *et al.* reveals that 4d ions such as  $\text{Ru}^{\text{III}}$  and  $\text{Mo}^{\text{V}}$  can provide the necessary strong magnetic exchange interactions to provide the means to design heterometallic 4f-4d SMMs with desirable properties.

## Conclusions

Three new  $\{\text{Ru}^{\text{III}}\text{Dy}^{\text{III}}\}$  “butterfly” complexes  $2_{\text{Dy}}$ ,  $3_{\text{Dy}}$  and  $4_{\text{Dy}}$  have been synthesised in order to enhance the blocking barrier for magnetic relaxation and to compare the results to those for our previously reported complex  $1_{\text{Dy}}$ . Two  $\text{Gd}^{\text{III}}$  analogues of the reported complex  $1_{\text{Dy}}$  (*viz.*  $1_{\text{Gd}}$ ) and of the new complex  $4_{\text{Dy}}$  ( $4_{\text{Gd}}$ ) were investigated in order to understand the mechanism of exchange interaction. Among all the  $\{\text{Ru}^{\text{III}}\text{Dy}^{\text{III}}\}$  complexes,  $3_{\text{Dy}}$  shows a blocking barrier of 45 K which is the highest value among such 4d-4f butterfly complexes. The SMM behaviour of complex  $3_{\text{Dy}}$  is attributed to its ligand-field environment which offers a stronger ligand-field<sup>35</sup> due to the presence of electron withdrawing groups on the benzoate ring combined with a higher  $J_{\text{Ru}\dots\text{Dy}}$  exchange coupling. Replacing the  $(\text{NO}_3)^-$  by MeOH in complex  $2_{\text{Dy}}$  leads to no slow relaxation under zero static field, despite it having similar exchange coupling to that of complex  $3_{\text{Dy}}$ . The smallest magnetic exchange in complex  $4_{\text{Dy}}$  results in an absence of a clear maximum in out-of-phase AC susceptibilities under a static zero magnetic field. Interestingly it was found the  $\text{Dy}^{\text{III}}\text{-Ru}^{\text{III}}$  exchange for  $3_{\text{Dy}}$  was strong enough to quench the ground state QTM, thus highlighting the promise for use of  $\text{Ru}^{\text{III}}$  ions in SMM design. However, compared to the earlier reported 3d-4f  $\{\text{Cr}^{\text{III}}\text{Dy}^{\text{III}}\}$  analogues, the exchange value for all the complexes ( $1_{\text{Dy}}\text{-}4_{\text{Dy}}$ ) has dropped significantly resulting in poorer SMM behaviour compared to their 3d analogues. This invariably suggests that both the number of unpaired electrons in the transition metal ions as well as the diffuse nature of the orbitals are required to enhance the exchange coupling; in this regard,  $\text{Re}^{\text{IV}}\dots\text{Ln}^{\text{III}}$  could be attractive targets as  $\text{Re}^{\text{IV}}$  is known to stabilize  $S = 3/2$  state and generally possess large negative zero-field splitting values as well.<sup>49,50</sup>

## Conflicts of interest

There are no conflicts to declare.

## Acknowledgements

This work was supported by an Australian Research Council Discovery grant to K. S. M. Part of this work was conducted using the MX1 beamline at the Australian Synchrotron, which is part of ANSTO. The authors acknowledge use of facilities within the Monash X-ray Platform. G. R. acknowledges DST/SERB for funding (No. CRG/2018/000430, DST/SJF/CSA-03/2018-10, SB/SJF/2019-20/12).

## References

- G. Christou, D. Gatteschi, D. N. Hendrickson and R. Sessoli, *MRS Bull.*, 2000, **25**, 66–71.
- R. Tiron, W. Wernsdorfer, N. Aliaga-Alcalde and G. Christou, *Phys. Rev. B: Condens. Matter Mater. Phys.*, 2003, **68**, 140407.
- J. D. Rinehart, M. Fang, W. J. Evans and J. R. Long, *Nat. Chem.*, 2011, **3**, 538–542.
- Y. Peng and A. K. Powell, *Coord. Chem. Rev.*, 2021, **426**, 213490.
- A. Chakraborty, J. Goura, P. Kalita, A. Swain, G. Rajaraman and V. Chandrasekhar, *Dalton Trans.*, 2018, **47**, 8841–8864.
- L. R. Piquer and E. C. Sañudo, *Dalton Trans.*, 2015, **44**, 8771–8780.
- S. K. Langley, D. P. Wielechowski, V. Vieru, N. F. Chilton, B. Moubaraki, B. F. Abrahams, L. F. Chibotaru and K. S. Murray, *Angew. Chem., Int. Ed.*, 2013, **52**, 12014–12019.
- S. K. Langley, N. F. Chilton, L. Ungur, B. Moubaraki, L. F. Chibotaru and K. S. Murray, *Inorg. Chem.*, 2012, **51**, 11873–11881.
- T. Gupta, M. F. Beg and G. Rajaraman, *Inorg. Chem.*, 2016, **55**, 11201–11215.
- S. A. Magee, S. Sproules, A. L. Barra, G. A. Timco, N. F. Chilton, D. Collison, R. E. Winpenny and E. J. McInnes, *Angew. Chem., Int. Ed.*, 2014, **53**, 5310–5313.
- F. Pointillart, K. Bernot, R. Sessoli and D. Gatteschi, *Chem. – Eur. J.*, 2007, **13**, 1602–1609.
- K. R. Vignesh, S. K. Langley, K. S. Murray and G. Rajaraman, *Chem. – Eur. J.*, 2017, **23**, 1654–1666.
- S. K. Langley, D. P. Wielechowski, V. Vieru, N. F. Chilton, B. Moubaraki, L. F. Chibotaru and K. S. Murray, *Chem. Sci.*, 2014, **5**, 3246–3256.
- Y. Peng, M. K. Singh, V. Mereacre, C. E. Anson, G. Rajaraman and A. K. Powell, *Chem. Sci.*, 2019, **10**, 5528–5538.
- G. Abbas, M. Ibrahim, S. F. Schmidt, E. Moreno-Pineda, C. E. Anson and A. K. Powell, *Polyhedron*, 2019, **158**, 255–261.
- S. K. Langley, D. P. Wielechowski, V. Vieru, N. F. Chilton, B. Moubaraki, L. F. Chibotaru and K. S. Murray, *Chem. Commun.*, 2015, **51**, 2044–2047.
- J. Rinck, G. Novitchi, W. Van den Heuvel, L. Ungur, Y. Lan, W. Wernsdorfer, C. E. Anson, L. F. Chibotaru and A. K. Powell, *Angew. Chem., Int. Ed.*, 2010, **49**, 7583–7587.

- 18 S. K. Singh, M. F. Beg and G. Rajaraman, *Chem. – Eur. J.*, 2016, **22**, 672–680.
- 19 M. M. Hanninen, A. J. Mota, R. Sillanpaa, S. Dey, G. Velmurugan, G. Rajaraman and E. Colacio, *Inorg. Chem.*, 2018, **57**, 3683–3698.
- 20 B. N. Figgis and M. A. Hitchman, *Ligand field theory and its applications*, Wiley-Vch, New York, 2000.
- 21 T. M. McPhillips, S. E. McPhillips, H.-J. Chiu, A. E. Cohen, A. M. Deacon, P. J. Ellis, E. Garman, A. Gonzalez, N. K. Sauter and R. P. Phizackerley, *J. Synchrotron Radiat.*, 2002, **9**, 401–406.
- 22 W. Kabsch, *J. Appl. Crystallogr.*, 1993, **26**, 795–800.
- 23 C. B. Hübschle, G. M. Sheldrick and B. Dittrich, *J. Appl. Crystallogr.*, 2011, **44**, 1281–1284.
- 24 M. Llunell, D. Casanova, J. Girera, P. Alemany and S. Alvarez, *SHAPE Version 2*, University of Barcelona, 2010.
- 25 J. Cirera, E. Ruiz and S. Alvarez, *Organometallics*, 2005, **24**, 1556–1562.
- 26 N. F. Chilton, R. P. Anderson, L. D. Turner, A. Soncini and K. S. Murray, *J. Comput. Chem.*, 2013, **34**, 1164–1175.
- 27 N. F. Chilton, *CC-fit*, The University of Manchester, UK, 2014, <http://www.nfchilton.com/cc-fit.html>.
- 28 K. R. Vignesh, D. I. Alexandropoulos, H. Xie and K. R. Dunbar, *Dalton Trans.*, 2020, **49**, 4694–4698.
- 29 S. K. Langley, K. R. Vignesh, K. Holton, S. Benjamin, G. B. Hix, W. Phonsri, B. Moubaraki, K. S. Murray and G. Rajaraman, *Inorganics*, 2018, **6**, 61.
- 30 D. Reta and N. F. Chilton, *Phys. Chem. Chem. Phys.*, 2019, **21**, 23567–23575.
- 31 F. Aquilante, J. Autschbach, R. K. Carlson, L. F. Chibotaru, M. G. Delcey, L. D. Vico, I. F. Galvan, N. Ferre, L. M. Frutos, L. Gagliardi, M. Garavelli, A. Giussani, C. E. Hoyer, G. L. Manni, H. Lischka, D. Ma, P. A. Malmqvist, T. Meller, A. Nenov, M. Olivucci, T. B. Pedersen, D. Peng, F. Plasser, B. Pritchard, M. Reiher, I. Rivalta, I. Schapiro, J. Segarra-Mart, M. Stenrup, D. G. Truhlar, L. Ungur, A. Valentini, S. Vancoillie, V. Veryazov, V. P. Vysotskiy, O. Weingart, F. Zapata and R. Lindh, *J. Comput. Chem.*, 2016, **37**, 506–541.
- 32 P. Å. Malmqvist, B. O. Roos and B. Schimmelpfennig, *Chem. Phys. Lett.*, 2002, **357**, 230–240.
- 33 B. Swerts, L. F. Chibotaru, R. Lindh, L. Seijo, Z. Barandiaran, S. Clima, K. Pierloot and M. F. Hendrickx, *J. Chem. Theory Comput.*, 2008, **4**, 586–594.
- 34 L. Ungur, W. Van den Heuvel and L. F. Chibotaru, *New J. Chem.*, 2009, **33**, 1224–1230.
- 35 L. Chibotaru and L. Ungur, in <http://www.molcas.org/documentation/manual/node105.html>.
- 36 L. Chibotaru and L. Ungur, *SINGLE\_ANISO and POLY\_ANISO*, University of Leuven, 2006.
- 37 M. J. Frisch, G. W. Trucks, H. B. Schlegel, G. E. Scuseria, M. A. Robb, J. R. Cheeseman, G. Scalmani, V. Barone, G. A. Petersson, H. Nakatsuji, X. Li, M. Caricato, A. V. Marenich, J. Bloino, B. G. Janesko, R. Gomperts, B. Mennucci, H. P. Hratchian, J. V. Ortiz, A. F. Izmaylov, J. L. Sonnenberg, D. Williams-Young, F. Ding, F. Lipparini, F. Egidi, J. Goings, B. Peng, A. Petrone, T. Henderson, D. Ranasinghe, V. G. Zakrzewski, J. Gao, N. Rega, G. Zheng, W. Liang, M. Hada, M. Ehara, K. Toyota, R. Fukuda, J. Hasegawa, M. Ishida, T. Nakajima, Y. Honda, O. Kitao, H. Nakai, T. Vreven, K. Throssell, J. A. Montgomery Jr., J. E. Peralta, F. Ogliaro, M. J. Bearpark, J. J. Heyd, E. N. Brothers, K. N. Kudin, V. N. Staroverov, T. A. Keith, R. Kobayashi, J. Normand, K. Raghavachari, A. P. Rendell, J. C. Burant, S. S. Iyengar, J. Tomasi, M. Cossi, J. M. Millam, M. Klene, C. Adamo, R. Cammi, J. W. Ochterski, R. L. Martin, K. Morokuma, O. Farkas, J. B. Foresman and D. J. Fox, *Gaussian 16, Rev. B.01*, Gaussian, Inc., Wallingford CT, 2016.
- 38 A. Becke, *J. Chem. Phys.*, 1993, **98**, 5648.
- 39 L. Noodleman, *J. Chem. Phys.*, 1981, **74**, 5737–5743.
- 40 L. Gagliardi, R. Lindh and G. Karlström, *J. Chem. Phys.*, 2004, **121**, 4494–4500.
- 41 T. Rajeshkumar and G. Rajaraman, *Chem. Commun.*, 2012, **48**, 7856–7858.
- 42 T. Rajeshkumar, S. K. Singh and G. Rajaraman, *Polyhedron*, 2013, **52**, 1299–1305.
- 43 M. K. Singh, T. Rajeshkumar, R. Kumar, S. K. Singh and G. Rajaraman, *Inorg. Chem.*, 2018, **57**, 1846–1858.
- 44 K. S. Pedersen, G. Lorusso, J. J. Morales, T. Weyhermüller, S. Piligkos, S. K. Singh, D. Larsen, M. Schau-Magnussen, G. Rajaraman and M. Evangelisti, *Angew. Chem., Int. Ed.*, 2014, **53**, 2394–2397.
- 45 M. Lines, *J. Chem. Phys.*, 1971, **55**, 2977–2984.
- 46 L. F. Chibotaru, L. Ungur and A. Soncini, *Angew. Chem., Int. Ed.*, 2008, **47**, 4126–4129.
- 47 L. F. Chibotaru, L. Ungur, C. Aronica, H. Elmoll, G. Pilet and D. Luneau, *J. Am. Chem. Soc.*, 2008, **130**, 12445–12455.
- 48 L. E. Darago, M. D. Boshart, B. D. Nguyen, E. Perlt, J. W. Ziller, W. W. Lukens, F. Furche, W. J. Evans and J. R. Long, *J. Am. Chem. Soc.*, 2021, **143**(22), 8465–8475.
- 49 S. K. Singh and G. Rajaraman, *Nat. Commun.*, 2016, **7**, 1–8.
- 50 J. M. Lillo, J. Faus, F. Lloret and M. Julve, *Coord. Chem. Rev.*, 2015, **289**, 215–237.